Unified description of the softening behavior of beta-metastable and alpha plus beta titanium alloys during hot deformation

Cecilia Poletti, Lionel Germain, Fernando Warchomicka, Martina Dikovits, Stefan Mitsche

Unified description of the softening behavior of beta-metastable and alpha+beta titanium alloys during hot deformation

Cecilia Poletti [a,*], Lionel Germain [b,c], Fernando Warchomicka [a], Martina Dikovits [a], Stefan Mitsche [d]

[a] Institute of Materials Science and Welding, Graz University of Technology, Austria
[b] Laboratoire d'Etude des Microstructures et de Mécanique des Matériaux (LEM3), UMR 7239, CNRS/Université de Lorraine, F-57045 Metz, France
[c] Laboratory of Excellence on Design of Alloy Metals for low-mAss Structures ('LabEx DAMAS'), Université de Lorraine, France
[d] Institute for Electron Microscopy and Nanoanalysis (FELMI), Graz University of Technology, Austria

ARTICLE INFO

Keywords:
Titanium alloys
Hot deformation
Parent phase reconstruction
Dynamic recovery
Load partition

ABSTRACT

In this work, we propose a unified description of the softening behavior of a β metastable alloy and Ti6Al4V alloy. In the first part we provide sound evidence that the hot deformation of Ti6Al4V of the beta phase above and below the beta transus temperature takes place solely by dynamic recovery at moderate strains, similarly to the behavior of the Ti5Al5Mo5V3Cr1Zr near-beta alloy. This study was possible due to the combination of the fast cooling rates achieved after controlled hot deformation and the reconstruction of the parent beta phase from electron backscattered diffraction measurements of the frozen alpha phase by using an innovative developed algorithm. The dynamic recovery as a common dynamic restoration behavior for Ti6Al4V and Ti5Al5Mo5V3Cr1Zr is described mathematically with a Derby type relationship of the subgrain size and the stress of the beta phase. A rule of mixture allows the determination of the load partition between the two allotropic phases.

1. Introduction

The deformation of metals at high temperatures involves different softening mechanisms such as dynamic recovery and dynamic recrystallization. These mechanisms produce softening during deformation that counteracts the hardening due to the formation of new dislocations needed for plastic deformation to proceed. The result is a decrement in the value of the global stress. In general, high stacking fault materials at high temperature experiences dynamic recovery (DRV) [1], followed by continuous dynamic recrystallization (cDRX) with increasing strain [2]. In the case of titanium alloys, the different allotropic phases can restore dynamically by different mechanisms. In β- and near β-titanium alloys it is generally accepted that the predominating softening mechanism of the β phase is DRV [3,4]. However, for the most used titanium alloy, i.e. Ti6Al4V (Ti64) alloy, the softening mechanism is not clearly established. It was reported to be discontinuous dynamic recrystallization (DDRX) by some authors [5,6] and DRV by others [7,8]. In any case, the modeling under each assumption is able to predict successfully the rheological behavior (DDRX in [9,10] and DRV in [11]) without taking into account the physical behaviour.

The identification of the softening mechanism is achieved usually by ex-situ analysis of the microstructure of deformed samples. Unfortunately, for materials undergoing allotropic transformations such as many α+β titanium alloys, the high temperature phase is not stable at room temperature and cannot be retained after cooling. Therefore, interpretation of the deformation behavior of high temperature stable phases is done without direct observation of the β substructure. Another difficulty arises from the experimental point of view. Indeed, it was demonstrated that static recrystallization of the β phase in Ti64 occurs within some seconds after deformation above the β-transus temperature (T_β) [12]. This may interfere with the interpretation of microstructures when quenching is not performed quickly after deformation. It is also possible to identify softening mechanisms using in-situ measurements. This has been done for titanium alloys and aluminides by different methods [13,14], although the microstructure features developed in the bulk cannot be quantified. Another aspect during hot deformation of titanium alloys is the role that the α phase plays in the load partition. Since both phases are different from the crystallographic as well as the chemical composition point of view, their different stacking fault energies influence their dynamic restoration mechanisms.

For materials that dynamically recrystallized, Derby [15] found that the relationship between the steady state grain size D_{ss} and

* Corresponding author.
E-mail address: cecilia.poletti@tugraz.at (C. Poletti).

flow stresses σ_{ss} can be correlated as follows:

$$\frac{\sigma_{ss}}{G} = K_1\left(\frac{D_{ss}}{b}\right)^{-p} \quad (1)$$

With G being the shear modulus and b the Burgers vector. While the K_1 value varies between 1 and 10 for metallic materials, the p exponent takes the value of 3/2 for most metals [15]. Some others authors found larger values of p [16], probably due to the non-steady state condition. Similarly, the relationship between the steady state subgrain sizes (δss) and flow stresses can be correlated by Eq. (1) with $p=1$ [17] , as found for a large amount of materials [18]

$$\frac{\sigma_{ss}}{G} = K_2\left(\frac{\delta_{ss}}{b}\right)^{-1} \quad (2)$$

Eq. (2) has shown some deviation of the experimental behavior as summarized for many materials in [19], and the K_2 was determined to be a function of the exponent p [18]. Furthermore, the situation of multiphase materials is more complex, and the correlation of the flow stress with the developed microstructure becomes difficult. When dealing with allotropic materials, the flow stress of each phase can be expressed in general by using a rule of mixtures, as done for composites [20]. In the case of $\alpha+\beta$ titanium alloys with globular α phase, this will be expressed as

$$\sigma = \sigma_\alpha f_\alpha + \sigma_\beta f_\beta \quad (3)$$

f being the phase fraction, and α and β referring to the phases. It was found, that at high temperatures this correlation is not necessarily applied, and then a modified rule of mixtures is proposed in [21], using adjustable n_1 and n_2 strengthening coefficients that are greater than 1

$$\sigma = n_1\sigma_\alpha f_\alpha + n_2\sigma_\beta f_\beta \quad (4)$$

In any case, the experimental validation of any correlation between the microstructure and the flow stress requires the characterization of micro and substructure developed at the deformation conditions.

The objectives of this work are to describe the restoration mechanism of the β-phase occurring in Ti64 below and above the T_β and to describe the flow behaviour by a load partition model. Therefore, the static recrystallization of the β phase is suppressed by in-situ water quenching after hot deformation. Afterwards, the crystal information of the martensite α' formed during cooling is used to reconstruct the parents of the β- phase by a novel algorithm. Finally, a common description of the restoration of Ti64 and a near-β Ti–5Al–5Mo–5V–3Cr–1Zr (Ti55531) alloys is developed in a Derby's type equation.

2. Methodology

2.1. Materials

The materials selected for the present work are a Ti64 and a Ti55531 alloy. Contrary to Ti64, Ti55531 retains the β phase at room temperature after cooling, allowing its crystallographic analysis by electron backscatter diffraction (EBSD) and thus, a comparison of similar microstructural behavior. The T_β of the Ti64 and Ti55531 are 1000 °C and 803 °C, respectively.

The as received materials were double melted, pre-forged, solution treated and aged below the T_β. The Ti55531 alloy was heat treated at the deformation temperature and kept to reach equilibrium and a fully recrystallized state [22]. The obtained microstructure consists in primary globular α phase embedded in β grains.

The commercial Ti6Al4V alloy presented a bimodal microstructure with primary α grains partially interconnected. Since the α grains were not 100% recrystallized during the cogging process, some grains elongated in the direction of the cogging were observed [23].

2.2. Hot compression tests.

Hot compression tests of Ti64 cylindrical samples of 10 mm diameter and 15 mm length were carried out at 930, 950 and 1030 °C at 0.01 and 1 s^{-1} of strain rate and up to 0.7 of global strain using a Gleeble® 1500 device. Samples were taken from the cogged ingot, and were compressed in the perpendicular direction with respect to cogging. The specimens were heated and held at 930 and 950 °C for 30 min and at 1030 °C for 10 min before deformation. The samples were immediately in situ water quenched after hot deformation with a cooling rate of 7000 K s^{-1} measured at the surface of the sample. Finite element simulations (DEFORM™ 2D) showed a cooling rate in the middle of the sample up to 500 °C of 200 K s^{-1}. The high cooling rate was achieved because the ohmic heating system heats only the sample while the chamber remains cold and because a water jet unit was used. Thus, static restoration of the β phase and diffusion controlled phase transformation were both suppressed to obtain a "pure" martensitic transformation during cooling.

The hot compression tests for the Ti55531 were carried out with the same device at temperatures between 743 °C and 843 °C, and strain rates from 0.001 to 10 s^{-1}, as described in [24,22]. For this alloy, the β phase was retained after the same water quenching procedure as used for Ti64 due to the large amount of β-stabilizers alloying elements.

The flow curves at high strain rates were corrected by the self-heating effect using general thermodynamic assumptions of the first law, and a constant Taylor–Quinney parameter of 0.8.

2.3. Metallographic analysis

Ti64 and Ti55531 deformed and water quenched samples were metallographically prepared. Specimens were cut parallel to the load axis and mechanically ground and polished. The final polishing step was done using 0.05 µm colloidal silica suspension (OPS). The EBSD-measurements were performed on a Zeiss-Ultra 55 equipped with a CCD Digiview camera from EDAX-TSL. An acceleration voltage of 20 kV and a beam current of 6.6 nA were used to obtain high quality pattern. The EBSD data were analyzed with the OIM analysis software v7.1 from EDAX. With an appropriate specimen preparation the fine α' phase was resolved with an average CI of 0.4 over all measured points. After data cleaning, grains were obtained by clustering pixels with a misorientation angle lower than 11°. High Angle Grain Boundaries (HAGB) were defined to have a misorientation angle larger or smaller than 11° and called grain boundaries, while Low Angle Grain Boundaries (LAGB) were defined below 11° and called subgrain boundaries.

Grain orientation dispersion (GROD) and Kernel average misorientation (KAM) maps [25] were used to distinguish subgrains and highly local misoriented zones, respectively. In a GROD map, each point is colored according to its disorientation angle with respect to the average orientation of the grain, and the color scale goes from blue for an angular deviation of 0° to red for 50°. The pixels of the orientation maps are colored with the classical inverse pole figures code wrt. The compression axis corresponds to the vertical direction in all pictures.

Finally, the β-subgrain size was obtained by the ASTM interception method [26] of the orientation and GROD maps. A mean value of a diameter was obtained for each combination of strain rate and temperature.

2.4. Parent reconstruction

The β-phase was reconstructed from the α orientations of EBSD maps with Merengue 2 software that uses a procedure based on [27] but with some recent improvements to account for the deformed β microstructure. This procedure assumes that the α′ crystallographic domains (i.e. the α′ needles) have a strict Burgers orientation relationship with their parent β grain. The procedure involves three steps. In the first step, the initial domains were identified. They correspond to adjacent pixels disoriented by an angle lower than 3°. Sometimes domains inherited from different parent may have a disorientation angle lower than 3°. To ensure a correct identification of domains, the Anti-Leak Grain Identification (ALGrId) [28] was applied using a disorientation angle threshold of 0.2°. In the second step, each domain and its first neighbors are considered. If most domains can be related to a unique β parent orientation with a tolerance angle around the Burgers relationship of 3°, a fragment of known β orientation is formed. In the last step, the domains not corresponding to these fragments were added recursively to adjacent fragments if they were related to the Burgers relation with a tolerance of 4°. The reconstructed β orientations were obtained with an angular resolution of ∼2°. The Burgers relation used was (110)β//(0001)α , [1–11] β//(11–20)α, which can be expressed as Euler angles: (45 90 5.265 or 45 90 35.265) depending of the convention used for hcp crystal reference frame. For microstructures deformed below T_β, the primary α were identified manually prior to the reconstruction of the β phase. The reconstruction was performed with a high reliability: 85% of the α′ had more than four different neighboring variants.

3. Experimental results

The flow curves of both materials for different temperature and strain rates are depicted in Fig. 1. Ti55531 showed steady state after an initial peak for samples deformed up to 0.1 s^{-1} and continuous softening at higher strain rate. In the case of Ti64, steady state flow was the predominant behavior in all the curves.

Fig. 2 shows the measured and reconstructed crystallographic orientation maps of Ti64 of deformed and water quenched specimens. The martensite α′ phase presents a typical needle shape structure (Fig. 2(a) and (c)). Although the high cooling rate achieved, a primary α- grain boundary was formed by diffusion in the sample deformed at 1 s^{-1} (indicated by an arrow). The preferred crystal orientations of α′ already allowed some distinction of prior β grains.

Fig. 2(b) and (d) shows the β phase reconstructed from (a) and (c), respectively. The reconstructed orientation maps revealed misorientations within β grains, serrated HAGB and subgrains. A homogeneous substructure was formed during deformation at the low strain rate, while heterogeneous misorientation distribution within the β-grain was observed at the highest strain rate. The increment in the misorientation towards the grain observed in Fig. 2(d) generated new HAGB. Similar microstructural features were already observed in hot deformed Ti55531 alloy [24,22] and are shown in Fig. 3 after deformation at 823 °C.

Grain orientation deviation maps (GROD) in Fig. 4 allowed a clear evaluation of the subgrain structure in the β phase. Both GROD maps of Ti55531 and of Ti64 samples deformed at high strain rates (Fig. 4(b) and (d)) show highly misoriented zones close to HAGB and at deformation bands. New grains were identified by low values of GROD.

Fig. 5 shows the original and reconstructed orientation maps of the Ti64 alloy after hot deformation for two different conditions below T_β. The microstructure is composed by deformed primary α, and martensite transformed from the β-phase during rapid cooling (Fig. 5(a) and (d)). There is neither distinction of the β prior grains, nor of its substructure. The primary α grains show a clear substructure after deformation at 930 °C and 0.1 s^{-1} and 950 °C and 1 s^{-1} in Fig. 5(b) and (e), respectively. Additionally, it is observed that the amounts of primary α phase at the deformation temperature are different, 0.40 and 0.28 respectively, and that the primary α phase elongates more markedly at higher strain rates [23]. The parent β phase reconstruction done in Fig. 5(c) and (f) reveal β grains and subgrains with low internal misorientation.

The GROD maps in Fig. 6(a) and (b) allows a better distinction of the subgrains for quantification. The β subgrain size was determined for the first time in a Ti64 as a function of the deformation parameters and the results are plotted together with the subgrain size of Ti55531 in Fig. 7. Two different symbols are used to identify the subgrains in the material after deformation in the single phase field, i.e. above the T_β, and in the α+β field. In general, the tendency shows that the β-subgrain size increases with increasing the temperature and decreasing the strain rate. The data for subgrain size for near-β titanium alloys appearing in table [29] is in good agreement with the values obtained in Fig. 7.

4. Modeling

4.1. Single phase model

The microstructural features can be correlated with the stress

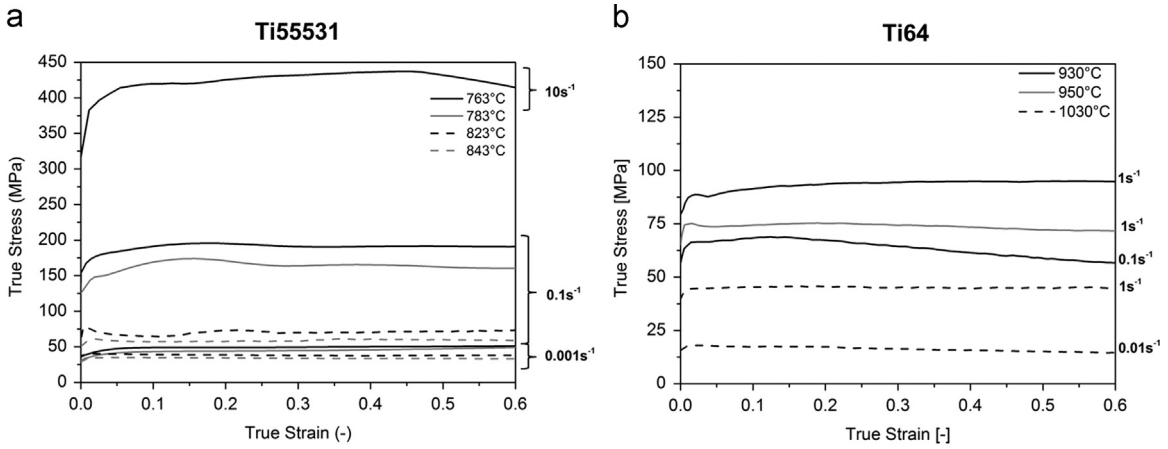

Fig. 1. Flow curves for different strain rates and temperature: (a) Ti55531 and (b) Ti64.

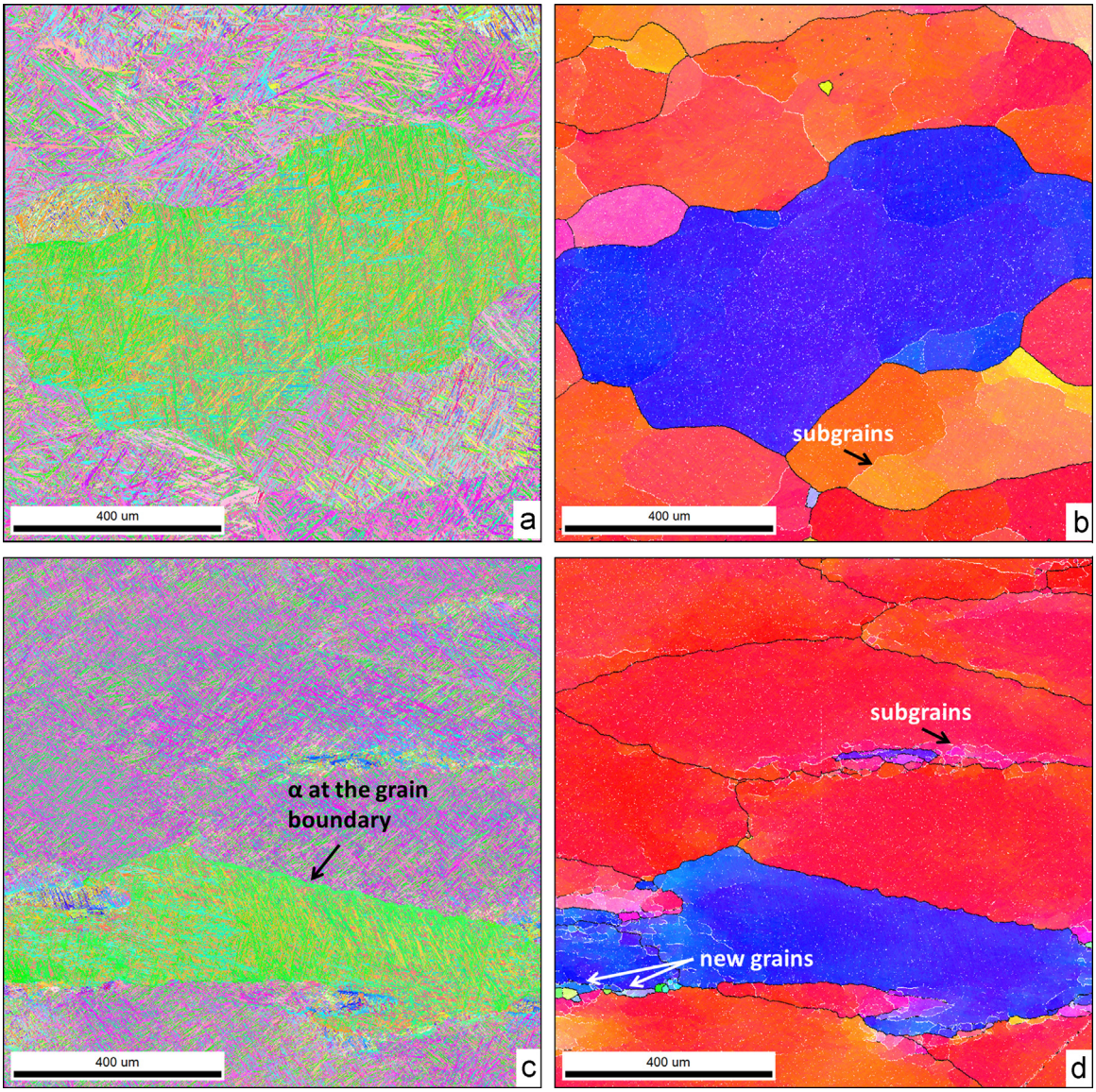

Fig. 2. Orientation maps of Ti64 (a), (c) deformed at 1030 °C, 0.01 and 1 s^{-1}, respectively, showing the martensitic α′ structure after deformation and water quenching. (b), (d) β-phase reconstructed from (a) and (c), respectively showing substructure within grains, HAGB in black, and LAGB in white.

values, using a form of Derby's type relationship (Eq. (2)). The shear moduli for the used materials are assumed to have a linear relationship with respect to the temperature (in °C) as follows: $G_{Ti64}=50-20.6$ T and $G_{Ti55531}=51.6-31.9$ T [30]. The Burgers vector value used is $b=0.00026$ μm [31]. The flow stresses normalized by G are plotted against the β subgrain sizes δ_β normalized by b in Fig. 8 for both materials deformed above T_β. The final obtained equation in the β field is

$$\frac{\sigma_{ss}}{G} = 3.42\left(\frac{\delta_\beta}{b}\right)^{-0.641} \tag{5}$$

Although the values of K_2 and p are within the expected values, the equation as written means that the total stress is produced by the formation of substructure. Instead, the total stress is a combination of many factors such as the strength of the pure metal, the solid solution strengthening, among others [32] plus the stress variation produced during the deformation. During dynamic recovery, the formation of the substructure occurs in the transient state as illustrated in Fig. 9. Therefore, if the starting microstructure is fully recrystallized, only the increment of the stress values represents the formation of dislocations and their annihilation and arrangement in subgrain boundaries. The following expression of the flow stress in the single-phase field adapted from [33] expresses this increment in the stress due to dynamic recovery, as illustrated with a dashed line in Fig. 9, where $\sigma_{ss}=\sigma_{DRV}$

$$\frac{\sigma_{ss}}{G} = \frac{\sigma_0+\Delta\sigma}{G} = \frac{\sigma_0}{G} + K_3\left(\frac{\delta_\beta}{b}\right)^{-p} \tag{6}$$

The stress σ_0 represents not only the yield stress of the pure metal, but also considers the contribution of precipitates and solution elements. Assuming that these two contributions remain constant during the deformation, σ_0 can be obtained from the experimental values of the stress at zero plastic strain. The increment in the stress $\Delta\sigma$ is related to the increment of the dislocation density. It can be considered that these dislocations form sharp subgrain boundaries at high temperatures. The correlation of the subgrain size with the increment in the stress is shown in Fig. 10, from which the following expression is found:

$$\frac{\Delta\sigma}{G} = 0.83\left(\frac{\delta_\beta}{b}\right)^{-0.68} \tag{7}$$

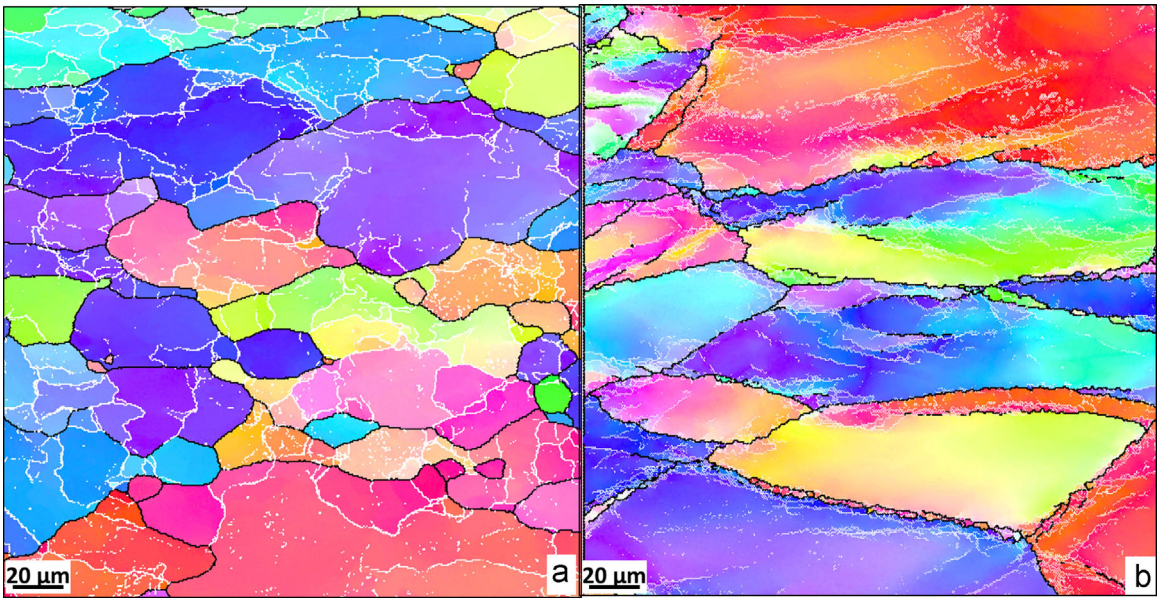

Fig. 3. Orientation maps of the retained β phase in Ti55531 after deformation at 823 °C and (a) 0.001 s^{-1} and (b) 1 s^{-1} showing homogeneous and heterogeneous substructure formation, respectively. Sample shown in (b) was not used for the subgrain size estimation.

4.2. Load partition model

For multiphase materials, Eq. (4) is used combined with the concepts shown above to determine the contribution of the α phase to the steady state flow stress and to the peak stress when deformation occurs in the two phase field

$$\sigma_{ss} = \sigma_{\alpha\,ss} f_\alpha + \sigma_{\beta\,ss} f_\beta \tag{8}$$

and

$$\sigma_{peak} = \sigma_{\alpha\,peak} f_\alpha + \sigma_{\beta\,peak} f_\beta \tag{9}$$

The volume fraction of the phases was determined experimentally [23,24]. Assuming that Eq. (5) can be applied for the two phase field then, the global stress in general is expressed as

$$\sigma = f_\alpha(\sigma_0 + \Delta\sigma_\alpha) + f_\beta(\sigma_0 + \Delta\sigma_\beta) \tag{10}$$

Again, σ_0 represents the contribution of phases, precipitates and alloying elements to the yield stress, it is determined from the stress at cero plastic deformation in the two phase deformation range, and it is assumed to be a contribution of both phases in a rule of mixtures way. Following the experimental observations, it is considered that the β phase form subgrains, thus applying Eq. (5) for the β behavior

$$\sigma_\beta = \sigma_0 + \Delta\sigma_\beta = \sigma_0 + GK_3\left(\frac{\delta_\beta}{b}\right)^{-p} \tag{11}$$

$$\sigma_\alpha = \sigma_0 + \Delta\sigma_\alpha \tag{12}$$

$\Delta\sigma_\alpha$ is used to represent a contribution related to the microstructural changes in α phase

The contribution of the phases to the total stress is obtained using the relationships (10) and (11)

$$\frac{\sigma}{G} = f_\alpha \frac{\sigma_0 + \Delta\sigma_\alpha}{G} + f_\beta\left[\frac{\sigma_0}{G} + K_3\left(\frac{\delta_\beta}{b}\right)^{-p}\right] \tag{13}$$

$\Delta\sigma_\alpha$ is calculated from Eq. (11), once σ_β is calculated from Eq. (10), assuming that K_3 and p values remain the same as in the single phase deformation (as shown in Eq. (6)). The stress increment value $\Delta\sigma_\alpha$ is related to the changes in the microstructure of the α phase, meaning it increases if the dislocation density within this phase increases.

The calculated steady state stresses in α and in the β phases are plotted in Fig. 11(a) using Eqs. (10) and (11).

Considering that β phase recovers, the value of σ_β at the peak stress and at steady state must be the same. Therefore, the same procedure described above was carried out to calculate σ_α at the peak stress σ_{peak} and the results are shown in Fig. 11(b).

5. Discussion

In the present work, evidence of DRV in the β-phase of Ti64 was proved thanks to the combination of the fast quenched microstructure after deformation and the crystallographic reconstruction of the β-phase parents using the EBSD data of the martensitic phase. The evidence of the DRV was given by the formation of subgrains and subgrain boundaries, similarly to that observed in diluted β-phase of near β-titanium alloys such as in Ti55531. No evidence of discontinuous recrystallization was observed in the β-phase. Instead, new grain formation by continuous lattice rotation was observed close to the prior β-grain boundaries in the samples deformed at high strain rate above the T_β and for both materials.

The use of a simple model to determine the dependency of the subgrain size with the stress was used. It was shown, that the exponent and the constant values used in the Derby type equation were closer to the literature values when using the increment in the stress produced by the formation of the substructure in β than when using the total stress value. On the other hand, the exponent p was found to be equal to 0.688, a value lower than the one expected by the formation of subgrains. One reason of discrepancy may be that subgrains are not completely polygonised, and that subgrains are more alike cells instead of sharp boundaries. This microstructure can be physically interpreted as not fully recovered. The cell size δ_c can be expressed as a function of the geometric necessary dislocations ρGND, and the misorientation θ as follows [34]:

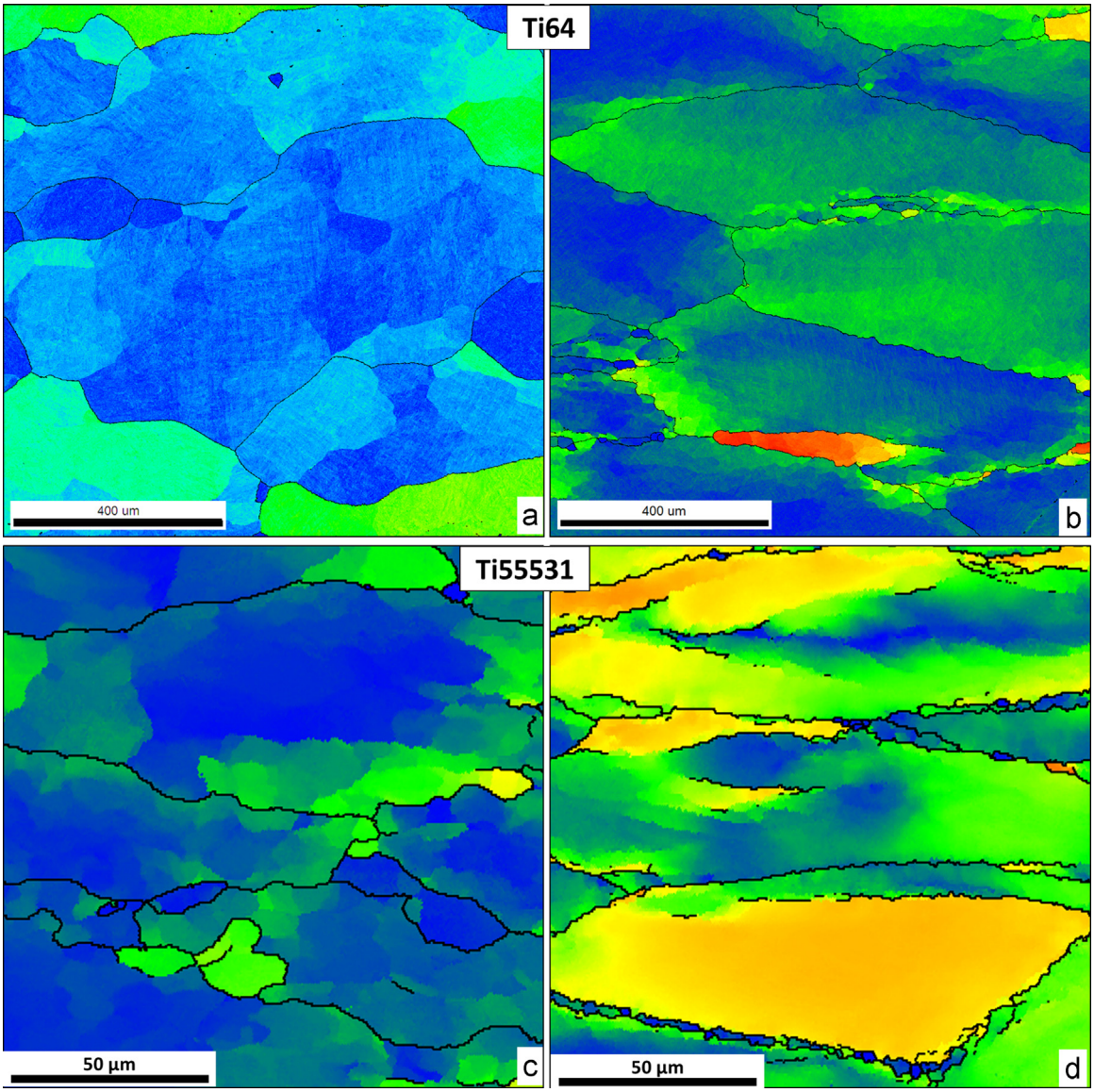

Fig. 4. Comparison of GROD maps obtained from: (a) and (b) reconstructed β parents in Ti64 for same deformation parameters as in Fig. 2, (c) and (d) from retained β phase in Ti55531 at deformation parameters of Fig. 3. Blue (0°) to red (50°). (For interpretation of the references to color in this figure legend, the reader is referred to the web version of this article.)

$$\rho_{GND} = \frac{3\theta}{\delta_c b} \tag{14}$$

The steady state stress can be expressed as a function of the dislocations density, and therefore, as a function of the cell size

$$\frac{\sigma}{G} = \frac{\sigma_0}{G} + K_4 b\sqrt{\rho_{GND}} = \frac{\sigma_0}{G} + K_4 b\sqrt{\frac{3\theta}{\delta_c b}} \tag{15}$$

where K_4 usually takes a value between 0.5 and 1. Considering that the misorientation remains more or less constant at moderate strains, then the interdependency of the cell size and the stress can be expressed as

$$\frac{\sigma}{G} = \frac{\sigma_0}{G} + K_4\sqrt{3\theta}\left(\frac{\delta_c}{b}\right)^{-0.5} \tag{16}$$

with $p=0.5$. Comparing the p value obtained in our work, which is between 0.5 and 1, we conclude that this should be as a result of a non-fully recovered microstructure.

The second reason of discrepancy of the p value in the Derby equation and the one found here could be the experimental method to determine the subgrain size, as pointed out by Orlová [19]. There is a general overestimation of the subgrain size by EBSD measurements due to the formation of low misoriented LAGB that cannot be detected by this experimental method, as detected by TEM [35,36], meaning that only LAGB with a disorientation angle well above the angular resolution of EBSD are detected. It should be mention, additionally, that the angular resolution of the reconstructed maps is even worse than that of measured orientations.

Subgrains formed in the β- phase in the presence of α-phase showed no large internal misorientations, as observed after deformation in the single phase field. This seems to be related to the role of the α-phase in the deformation of the selected materials and is corroborated by Kernel maps. Fig. 12 shows local Kernel maps of the cubic phase (a) and the hexagonal phase (b) of a Ti55531 sample deformed at 763 °C and 10 s^{-1}. While large misorientations developed within the α phase, homogenously distributed subgrains free of misorientations were observed. When plotting the Kernel map for the hexagonal phase of a Ti64 sample deformed at 930 °C and 1 s^{-1}(c), deformation bands and

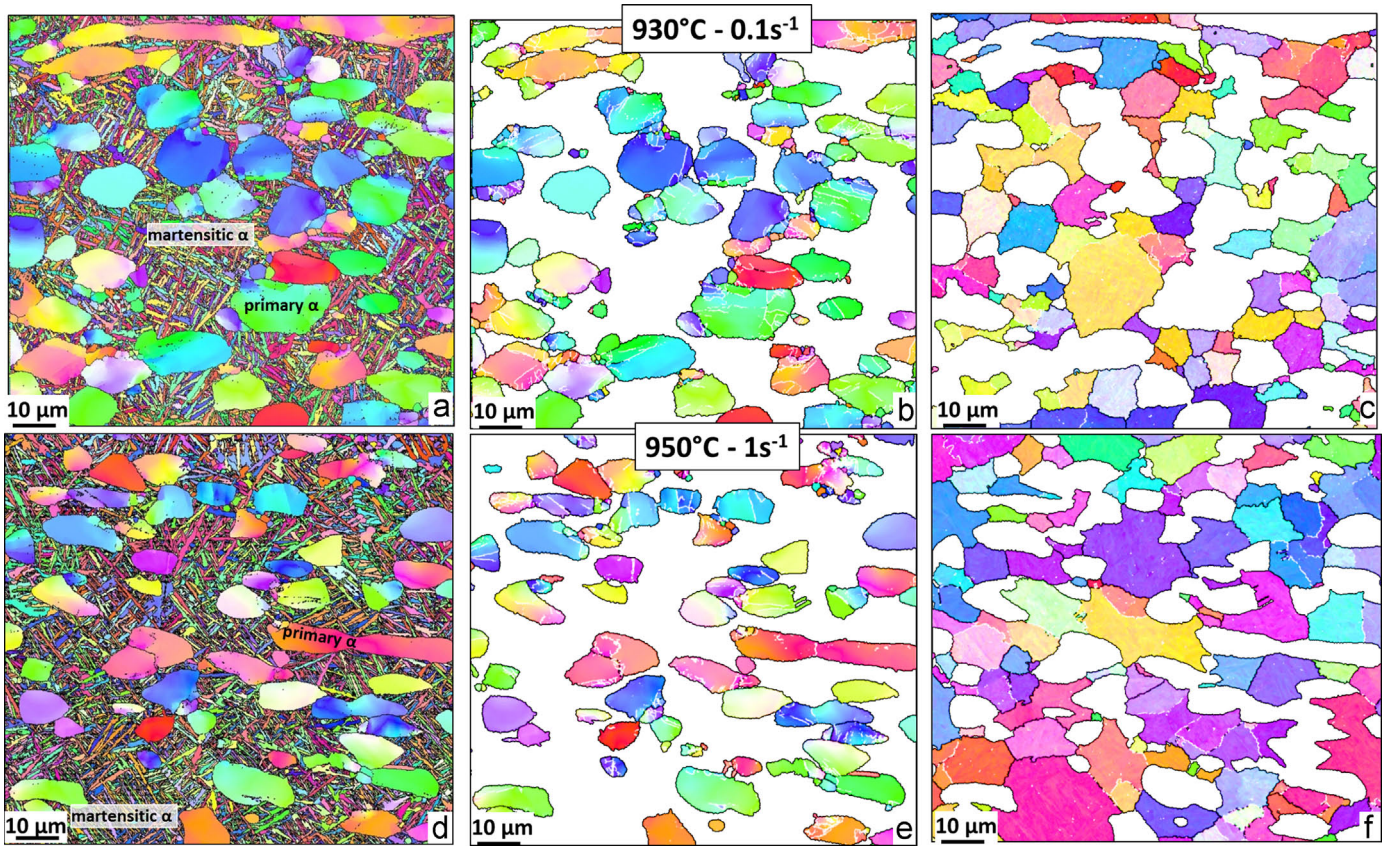

Fig. 5. Orientation maps of Ti64 after deformation below T_β and water quenching showing (a) and (d) the EBSD measurement of both primary and martensitic α-phases. (b) and (e) Separation of primary α grains and (c) and (f) reconstructed β after martensitic α-phase data treatment.

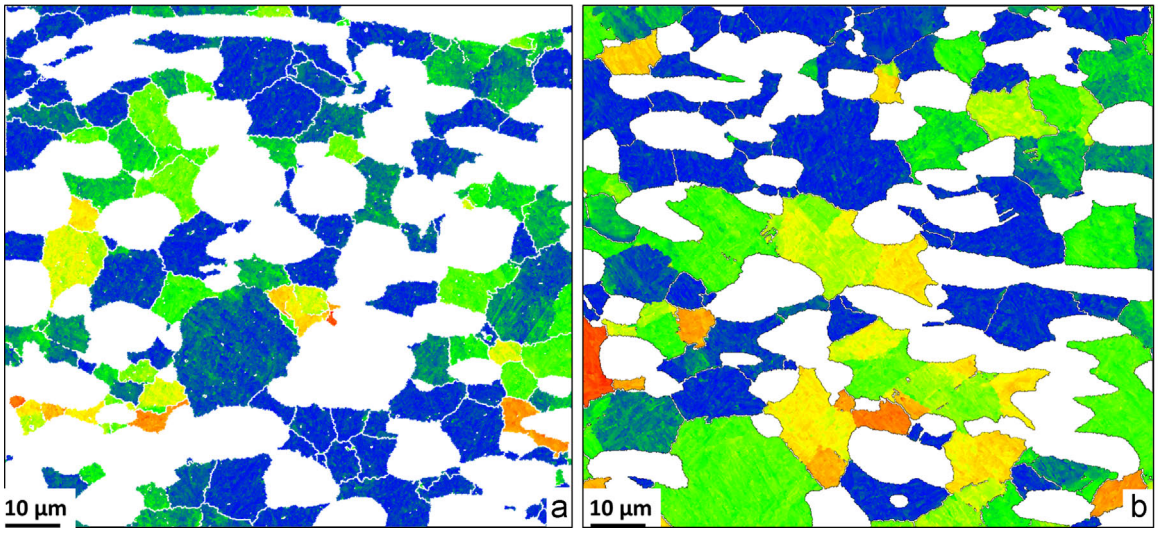

Fig. 6. GROD maps obtained from reconstructed β parents in Ti64 (a) and (b) corresponding to same deformation parameters as in Fig. 5, (a) and (d), respectively. Blue (0°) to red (50°) scale. (For interpretation of the references to color in this figure legend, the reader is referred to the web version of this article.)

inhomogeneous local misorientation were determined. Since the Kernel data can be correlated directly with the density of geometrically necessary dislocations [37], it can be deduced that the dislocation density in α is heterogeneously distributed, provoking fragmentation of the grains, as reported in [38,23]. This fragmentation and rotation of the α-phase in a more convenient orientation with respect to the load is responsible of the softening observed in the flow curves [39].

Since the calculation of the stress in β-phase was extrapolated from the single phase field into the two phase field, the interaction of the phases was not taken into account. Although Fig. 11 (b) reveals, that the hexagonal α phase strengthens the material, since in most of the cases σ_α is larger than σ_β, an underestimation of the stress values in α must occur. Fig. 13 was obtained plotting the σ_α values in as a function of the strain rate and the amount of primary α. It can be deduced, that by decreasing the amount of primary α, this phase deforms less and behaves as a hard phase in a soft matrix. Therefore, it pins low angle as well as high angle

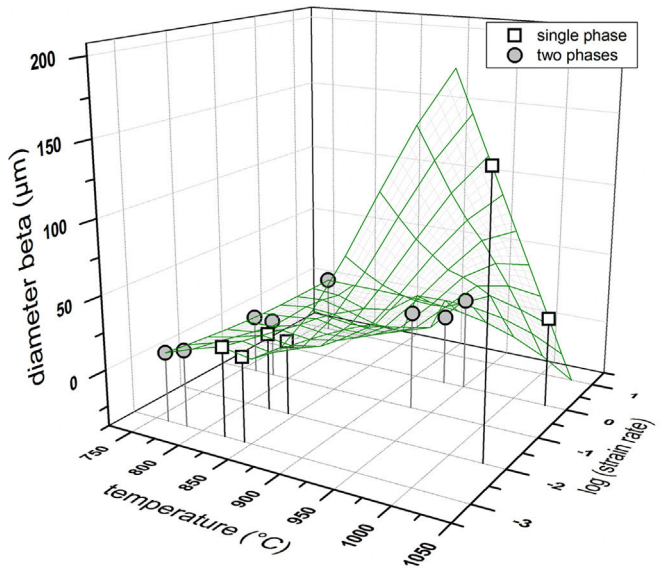

Fig. 7. Measured β-subgrain diameter after deformation above (open square) and below (circles) β-transus temperature.

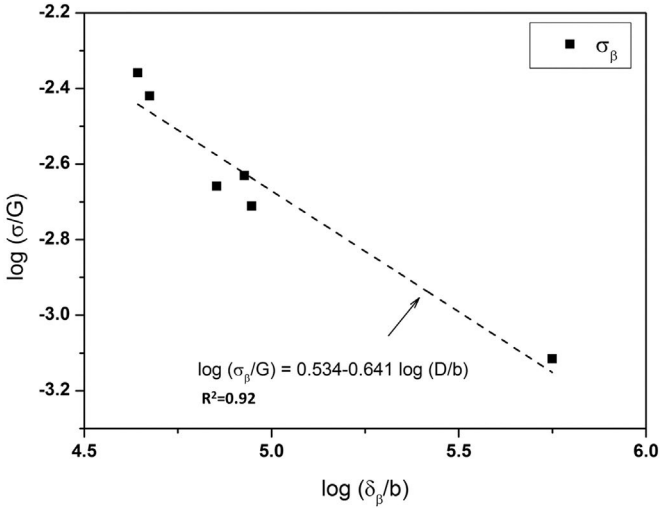

Fig. 8. Relationship between stress normalized by the shear modulus and β-subgrain size normalized by the burgers vector of samples deformed above T_β.

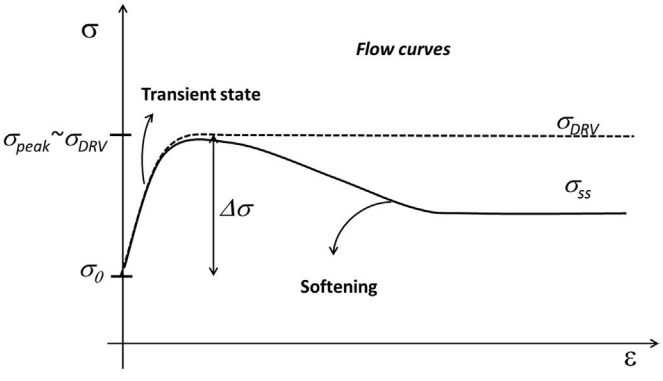

Fig. 9. Flow curves concept used for the model.

grain boundaries, strengthening the whole material. The pinning effect is evident at very low amount of hexagonal phase. This is illustrated by the Taylor factor map (Fig. 14) calculated considering active the slip systems {110}, {112} and {123} in the β-phase [30] in

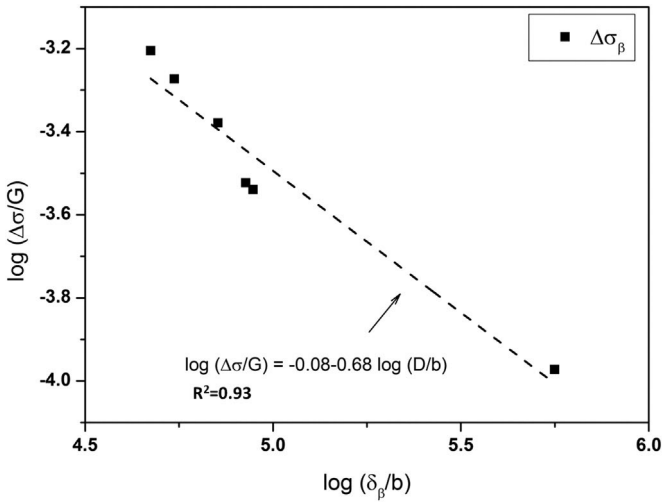

Fig. 10. Relationship between incremental stress normalized by the shear modulus and β-subgrain size normalized by the burgers vector of samples deformed above T_β.

Ti55531 after deformation at 783 °C and 0.001 s^{-1} of strain rate. The CRSS value used was 1, according to what was reported for similar crystal structures [40,41]. The dark colors with lower Taylor values are related to easily formable regions due to the combination of crystal orientation and load direction. The arrows indicate the boundaries mobility direction.

The increment of dislocation density in the α phase during deformation can be correlated to the increment of the stress in the α phase. This value is given by $\Delta\sigma_\alpha$ that is a function of the strain rate and the temperature. Fig. 15 shows this correlation at the peak stress and at the steady state stresses that can be mathematically expressed as

$$\Delta\sigma_{\alpha\,ss} = -3195 + \frac{3.9\cdot10^6}{T} + 52.4\ln\dot{\varepsilon} \tag{17}$$

$$\Delta\sigma_{\alpha\,peak} = -3985 + \frac{4.9\cdot10^6}{T} + 76\ln\dot{\varepsilon} \tag{18}$$

In general, it can be concluded that the stress increment in the α phase will be larger at higher strain rates and lower temperatures due to less dynamic restoration.

6. Conclusions

This work was carried out to elucidate the behaviour of the β-phase in two titanium alloys with an initial bimodal microstructure, as well as to find a common correlation of the developed microstructure with the strain rate and temperature. While the analysis of the β phase could be done from the EBSD measurements in the near-β Ti55531 titanium alloy, almost no trace of the β-phase could be identified after deformation and cooling in the Ti64 titanium alloy due to the martensitic transformation. Therefore, and for the first time, the substructure of its β phase could be reconstructed and analyzed to get clear information of the restoration mechanism.

From the exposed above, we conclude that:

1. The fast cooling rate and the reconstruction of the β-phase are essential to understand the deformation mechanisms taking place during hot deformation of α+β titanium alloys.
2. The use of GROD maps facilitates the understanding of the crystallographic evolution within grains.

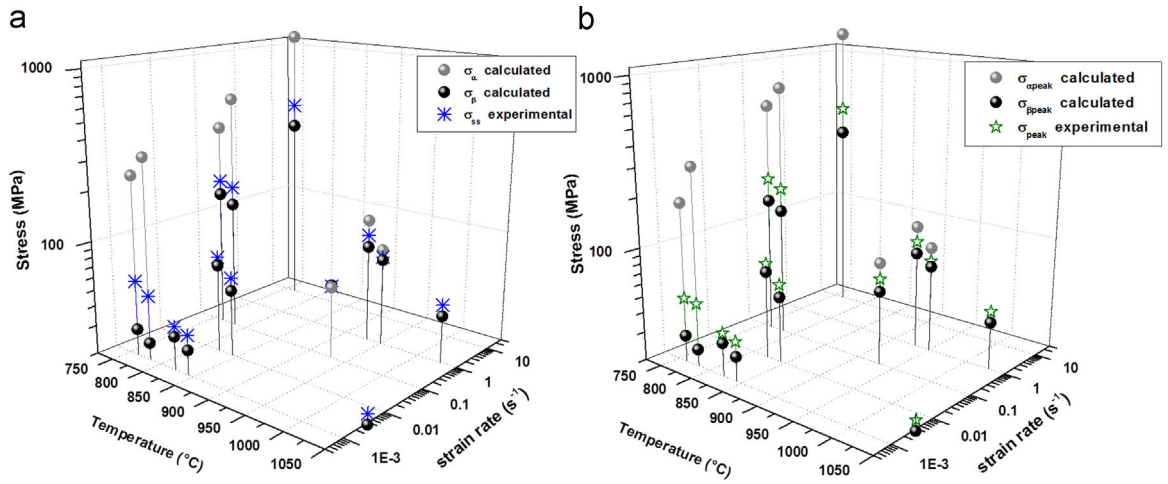

Fig. 11. (a) steady state and (b) peak stresses calculated for the α and β phases compared with the experimental values.

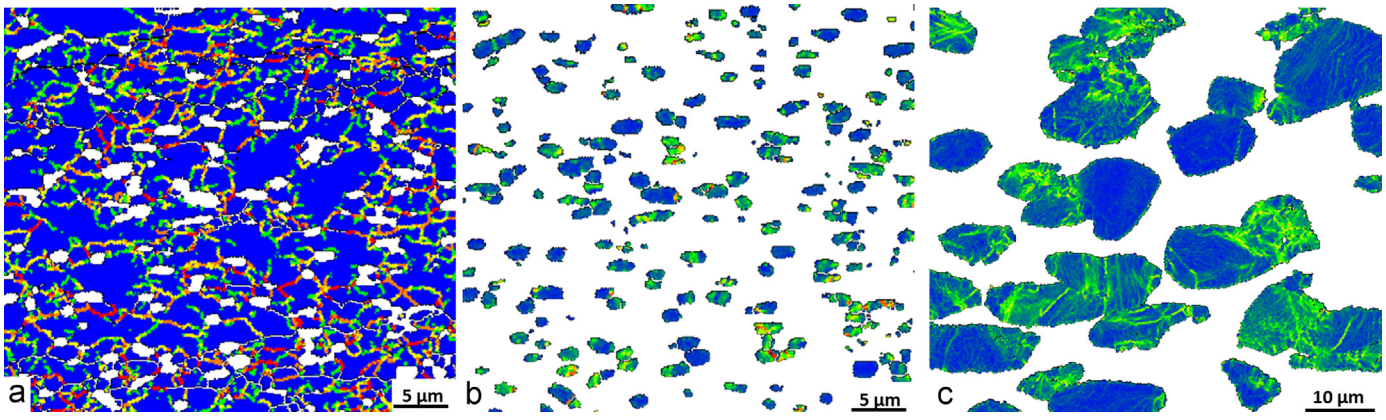

Fig. 12. Kernel map samples deformed below T_β showing the local misorientation of (a) and (b) Ti55531, (a) in β and (b) in α phases and of (c) Ti64 in the α phase. Misorientation calculated between 0° (blue) and 5° (red). (For interpretation of the references to color in this figure legend, the reader is referred to the web version of this article.)

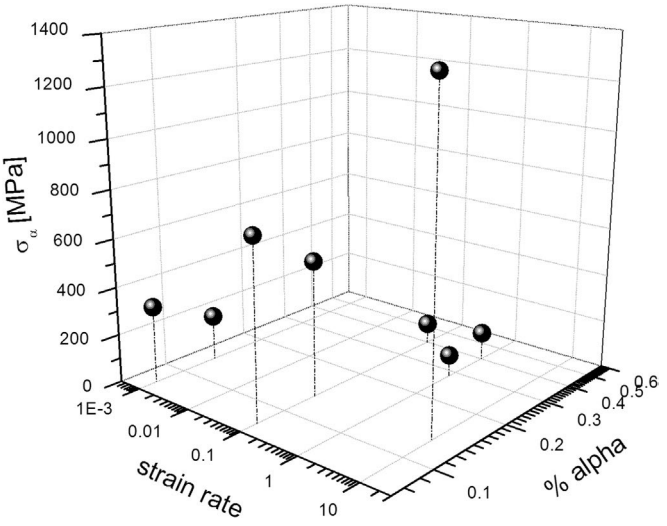

Fig. 13. Stresses in α as a function of the amount of α (in vol%) and the strain rate.

3. The reconstructed β-phase shows not only the shape of β grains, but also the formation of substructures and the local misorientation within them, are a clear sign of dynamic recovery. There is no evidence of discontinuous DRX at the studied conditions.

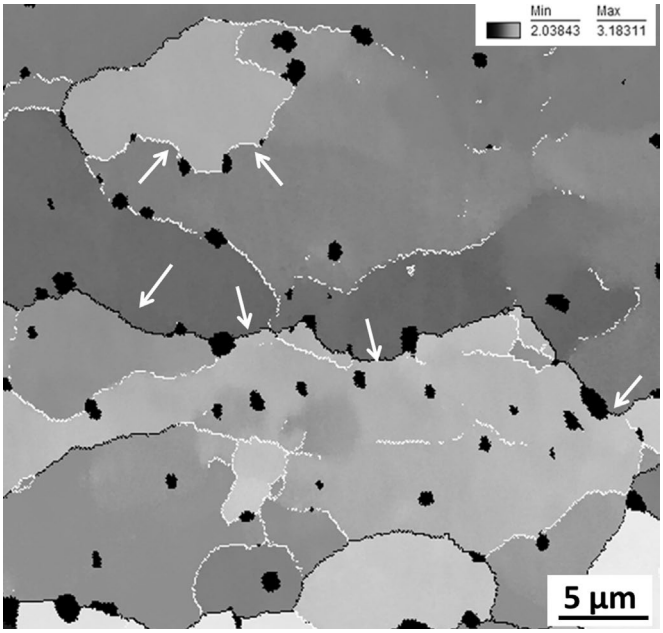

Fig. 14. Taylor factor map in the β-phase of Ti55531, showing pinning effect of the α phase in the high angle (white) and low angle grain boundaries.

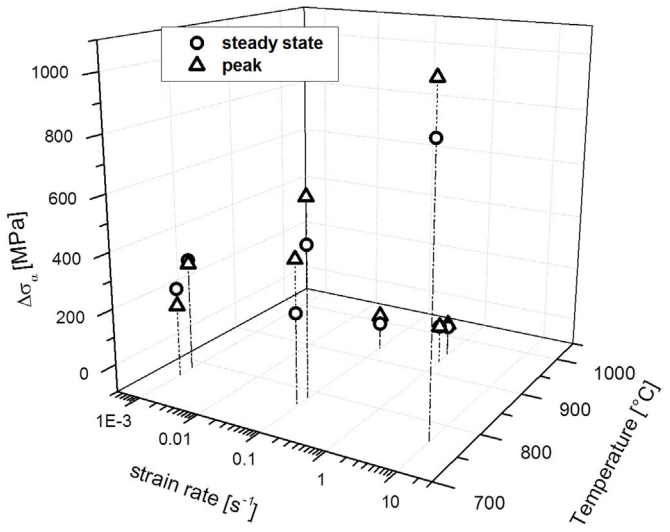

Fig. 15. Increment of the stress value in α as a function of the temperature and the strain rate.

4. Similar deformation mechanisms take place in the β-phase of both studied alloys: DRV followed by cDRX at high strain rate and DRV solely at low and moderate strain rates.
5. Stress and substructure size can be correlated by a Derby expression form. A more physical description is done, when the increment and re-arrangement in the dislocation density is considered as the only mechanism to form subgrains. Since the changes in the dislocation density is not given by the total stress, but by the increment in the stress, the subgrain size should be correlated only with this increment of the stress.
6. A *p* exponent value of 0.7 in the modified Derby equation was found as a result of cell formation and limitation of the EBSD technique.
7. The stress in the two phase field was analysed using a rule of mixtures that did not take into account interactions between the phases. The model can be used to describe the dependency of the stress in the hexagonal phase as a function of the strain rate and phases amount. Low amounts of α phase support large stresses and pin β-boundary migration.

Acknowledgments

The work was partially supported by the Austrian Science Fund (FWF) under the Project N° (P22238-N22) and by the Austrian Research Promotion Agency (FFG) under the Project N° 815855, in cooperation with Böhler Schmiedetechnik GmbH & Co KG. The authors thank to USTEM at TU Vienna for the EBSD facilities.

References

[1] M.R. Drury, F.J. Humphreys, The development of microstructure in Al–5% Mg during high temperature deformation, Acta Metall. 34 (11) (1986) 2259–2271, http://dx.doi.org/10.1016/0001-6160(86)90171-9.
[2] S. Gourdet, F. Montheillet, An experimental study of the recrystallization mechanism during hot deformation of aluminium, Mater. Sci. Eng. A 283 (1-2) (2000) 274–288.
[3] M. Jackson, R. Dashwood, L. Christodoulou, H. Flower, The microstructural evolution of near beta alloy Ti–10V–2Fe–3Al during subtransus forging, Metall. Mater. Trans. A: Phys. Metall. Mater. Sci. 36 (5) (2005) 1317–1327.
[4] F. Montheillet, D. Dajno, N. Come, E. Gautier, A. Simon, P. Audrerie, A.-M. Chaze, Ch Levaillant, Titanium '92: Science and Technology, TMS (1993), p. 1347–1354.
[5] Y.V.R.K. Prasad, T. Seshacharyulu, S.C. Medeiros, W.G. Frazier, A study of beta processing of Ti–6Al–4V: is it trivial, J. Eng. Mater. Technol. Trans. ASME 123 (3) (2001) 355–360, http://dx.doi.org/10.1115/1.1372708.
[6] V. Venkatesh, M. Kamal, J. Fanning, Ti-2007: Sci. Technol. JIM (2007) 503.
[7] N.-K. Park, J.-T. Yeom, Y.-S. Na, Characterization of deformation stability in hot forging of conventional Ti-6Al-4V using processing maps, J. Mater. Process. Technol. 130–131 (2002) 540–545, http://dx.doi.org/10.1016/S0924-0136(02)00801-4.
[8] A. Majorell, S. Srivatsa, R.C. Picu, Mechanical behavior of Ti–6Al–4V at high and moderate temperatures-Part I: experimental results, Mater. Sci. Eng. A 326 (2) (2002) 297–305, http://dx.doi.org/10.1016/S0921-5093(01)01507-6.
[9] H. Li, C. Wu, H. Yang, Crystal plasticity modeling of the dynamic recrystallization of two-phase titanium alloys during isothermal processing, Int. J. Plast. 51 (2013) 271–291, http://dx.doi.org/10.1016/j.ijplas.2013.05.001.
[10] H. Yang, P.F. Gao, X.G. Fan, H.W. Li, Z.C. Sun, H. Li, L.G. Guo, M. Zhan, Y.L. Liu, Some advances in plastic forming technologies of titanium alloys, Proc. Eng. 81 (C) (2014) 44–53, http://dx.doi.org/10.1016/j.proeng.2014.09.127.
[11] R.C. Picu, A. Majorell, Mechanical behavior of Ti–6Al–4V at high and moderate temperatures – Part II: constitutive modeling, Mater. Sci. Eng. A 326 (2) (2002) 306–316, http://dx.doi.org/10.1016/S0921-5093(01)01508-8.
[12] F. Warchomicka, C. Poletti, M. Stockinger, Microstructural characterization of hot deformed Ti–6A1–4V, in: Ti 2011 – Proceedings of the 12th World Conference on Titanium, vol. 1, 2012, pp. 729–732.
[13] David Canelo Yubero (Ph.D. thesis). TU Vienna, 2014.
[14] T. Schmoelzer, K.-D. Liss, C. Kirchlechner, S. Mayer, A. Stark, M. Peel, H. Clemens, An in-situ high-energy X-ray diffraction study on the hot-deformation behavior of a β-phase containing TiAl alloy, Intermetallics 39 (2013) 25–33, http://dx.doi.org/10.1016/j.intermet.2013.02.016.
[15] B. Derby, The dependence of grain size on stress during dynamic recrystallization, Acta Metall. Mater. 39 (5) (1991) 955–962, http://dx.doi.org/10.1016/0956-7151(91)90295-C.
[16] J. Xing, H. Soda, X. Yang, H. Miura, T. Sakai, Ultra-fine grain development in an AZ31 magnesium alloy during multi-directional forging under decreasing temperature conditions, Mater. Trans. 46 (7) (2005) 1646–1650, http://dx.doi.org/10.2320/matertrans.46.1646.
[17] S. Takeuchi, A.S. Argon, Steady-state creep of alloys due to viscous motion of dislocations, Acta Metall. 24 (10) (1976) 883–889, http://dx.doi.org/10.1016/0001-6160(76)90036-5.
[18] S.V. Raj, G.M. Pharr, A compilation and analysis of data for the stress dependence of the subgrain size, Mater. Sci. Eng. 81 (C) (1986) 217–237, http://dx.doi.org/10.1016/0025-5416(86)90265-X.
[19] A. Orlová, On the applied stress dependence of the subgrain size, Mater. Sci. Eng. A 220 (1–2) (1996) 117–122, http://dx.doi.org/10.1016/S0921-5093(96)10432-9.
[20] T.W. Clyne, P.J. Withers, An Introduction to Metal Matrix Composites, Cambridge University Press, Cambridge, 1993.
[21] J. Luo, M. Li, X. Li, Y. Shi, Constitutive model for high temperature deformation of titanium alloys using internal state variables, Mech. Mater. 42 (2) (2010) 157–165, http://dx.doi.org/10.1016/j.mechmat.2009.10.004.
[22] F. Warchomicka, C. Poletti, M. Stockinger, Study of the hot deformation behaviour in Ti–5Al–5Mo–5V–3Cr–1Zr, Mater. Sci. Eng. A 528 (28) (2011) 8277–8285, http://dx.doi.org/10.1016/j.msea.2011.07.068.
[23] F. Warchomicka, C. Poletti, M. Stockinger, H.P. Degischer, Determination of the mechanism of restoration in subtransus hot deformation of Ti–6Al–4V, Mater. Sci. Forum 706–709 (2012) 252–257, http://dx.doi.org/10.4028/www.scientific.net/MSF.706-709.252.
[24] M. Dikovits, C. Poletti, F. Warchomicka, Deformation mechanisms in the near-β titanium alloy Ti-55531, Metall. Mater. Trans. A: Phys. Metall. Mater. Sci. 45 (3) (2014) 1586–1596, http://dx.doi.org/10.1007/s11661-013-2073-4.
[25] Orientation Imaging Microscopy (OIM™) Data Analysis Manual.
[26] ASTM E112 – E113. Standard Test Methods for Determining Average Grain Size.
[27] L. Germain, N. Gey, R. Mercier, P. Blaineau, M. Humbert, An advanced approach to reconstructing parent orientation maps in the case of approximate orientation relations: application to steels, Acta Mater. 60 (11) (2012) 4551–4562, http://dx.doi.org/10.1016/j.actamat.2012.04.034.
[28] L. Germain, D. Kratsch, M. Salib, N. Gey, Identification of sub-grains and low angle boundaries beyond the angular resolution of EBSD maps, Mater. Charact. 98 (2014) 66–72, http://dx.doi.org/10.1016/j.matchar.2014.10.007.
[29] J. Da Costa Teixeira, B. Appolaire, E. Aeby-Gautier, S. Denis, F. Bruneseaux, Modeling of the effect of the β phase deformation on the α phase precipitation in near-β titanium alloys, Acta Mater. 54 (16) (2006) 4261–4271.
[30] DEFORM™ 2DDatabase.
[31] Titanium Gerd Lütjering, James C. Williams, Springer Science & Business Media, 17th August 2007.
[32] E. Voce, The relationship between stress and strain for homogeneous deformation, J. Inst. Met. 74 (1948) 537–562.
[33] F.R. Castro-Fernandez, C.M. Sellars, Relationship between room-temperature proof stress, dislocation density and subgrain size, Philos. Mag. A: Phys. Condens. Matter Struct. Defects Mech. Prop. 60 (4) (1989) 487–506.
[34] Recrystallization and Related Annealing Phenomena (Second Edition). F.J. Humphreys and M. Hatherly, 2004.
[35] M. Cabibbo, W. Blum, E. Evangelista, M.E. Kassner, M.A. Meyers, Transmission electron microscopy study of strain-induced low- and high-angle boundary development in equal-channel angular-pressed commercially pure aluminum, Metall. Mater. Trans. A: Phys. Metall. Mater. Sci. 39 (1) (2008) 181–189, http://dx.doi.org/10.1007/s11661-007-9350-z.
[36] C. Poletti, T. Wójcik, C. Sommitsch, Hot deformation of AA6082 containing fine intermetallic particles, Metall. Mater. Trans. A: Phys. Metall. Mater. Sci. 44 (3) (2013) 1577–1586, http://dx.doi.org/10.1007/s11661-012-1487-8.
[37] E. Demir, D. Raabe, N. Zaafarani, S. Zaefferer, Investigation of the indentation size effect through the measurement of the geometrically necessary dislocations beneath small indents of different depths using EBSD tomography, Acta Mater. 57 (2) (2009) 559–569, http://dx.doi.org/10.1016/j.actamat.2008.09.039.
[38] S. Zherebtsov, M. Murzinova, G. Salishchev, S.L. Semiatin, Spheroidization of the

lamellar microstructure in Ti–6Al–4V alloy during warm deformation and annealing, Acta Mater. 59 (10) (2011) 4138–4150, http://dx.doi.org/10.1016/j.actamat.2011.03.037.
[39] T.R. Bieler, S.L. Semiatin, The origins of heterogeneous deformation during primary hot working of Ti–6Al–4V, Int. J. Plast. 18 (9) (2002) 1165–1189, http://dx.doi.org/10.1016/S0749-6419(01)00057-2.
[40] D. Daniel, J.J. Jonas, Texture and anisotropy of plastic properties in deep drawing steels, Text. Microstruct. 14–18 (1991) 1165–1171.
[41] J. Hamada., H. Inoue, Texture and planar anisotropy of *r*-value in duplex stainless steel sheet, Mater. Trans. 51 (4) (2010) 644–651.